BIOMATERIALS FOR THE CENTRAL NERVOUS SYSTEM

Contract No. NO1-NS-1-2338

Quarterly Progress Report #4

January 30, 2002

The University of Michigan and
The University of Utah

David C. Martin and Patrick A. Tresco

Quarterly Progress to:	National Institute of Health
Contract Monitor:	William Heetderks, Ph.D.
Research Contract	"Biomaterials for the Central Nervous System"
Contract No.	NO1-NS-1-2338
Principal Investigators:	David C. Martin and Patrick A. Tresco
Date:	October 31, 2002

Overview

This report is a summary of our activity in the fourth quarter of our new contract, corresponding to the period from July 31, 2002 to October 31, 2002. We discuss our work to develop polymer films for the surface modification of neural prosthetic devices and the *in vitro* and *in-vivo* testing of these modified electrodes.

In this quarterly report we first discuss results from the Martin group on the development of nanostructured conducting polymer (polypyrrole) coatings, using block copolymer and Nuclepore membranes. We also discuss refinements to our techniques for growing polypyrrole within alginate hydrogels. We also show that larger-scale porosity can be introduced into the hydrogels by freezing either in a conventional freezer or with liquid nitrogen. The subsequent polymerization of polypyrrole in the lyophilized gels is quite different than that seen in the intact hydrogels. We then present work from the Tresco group to examine the biological response of the coated probes.

Aspects of this work were presented at the recent Neural Prosthesis meeting in Bethesda, MD. Personell attending the meeting this year were Prof. David Martin, Prof. Patrick Tresco, Dr. Yinghong Xiao, Dr. Junyan Yang, Mr. Donghwan Kim, and Mr. Mohammad Abidian.

Surface Modification of Neural Prostheses with Nanostructured Conducting Polymer Coatings

Abstract

We successfully demonstrated a method to rapidly and reliably fabricate nanostructured conducting polymer coatings on the electrode probes using nanoporous membranes as templates. Nanostructured coatings, such as, nanomushrooms and nanohairs, were electrochemically polymerized on the electrode site. The coating thickness, the size of nanomushrooms and nanohairs could be tailored by changing current density, deposition time, pore size and thickness of membranes. The morphologies and electrical properties of coatings have been investigated.

Introduction

Micromachined neural prosthetic devices facilitate the functional stimulation of and recording from the central nervous system (CNS). These devices have been fabricated to consist of silicon shanks that have gold sites along their surfaces. Our goal is to improve the biocompatibility and long-term performance of the neural prosthetic probes when they are implanted chronically in the brain. In our most recent efforts [1-2], we have established that electrochemical polymerization can be used to deposit fuzzy conducting polymer coatings, such as polypyrrole (PPy), poly(3, 4-ethylenedioxythiophene) (PEDOT) and PEDOT derivates, specifically on the electrode sites. For neural prosthetic devices that are intended for long term implantation, we need to develop surfaces that provide intimate contact and promoting efficient signal transport at the interface of microelectrode array and brain tissue.

Recently, nanostructured (nanotube and nanofiber) materials have attracted attention because of their novel, unique properties and a series of applications in chemistry, physics, electronics, optics, materials science and biomedical science. Conducting polymers are promising in this area due to their long conjugated length and metallike conductivity. In general, only granular or fibrillar morphology was observed for conducting polymers synthesized by conventional chemical or electrochemical polymerization although the morphology depends on the polymerization method and conditions.

However, a series of papers concerning the nanostructured conducting polymers have been published. Among the different strategies reported in the literature, the "template synthesis" method proposed by Martin et al [3] is an elegant approach to synthesize nanotube and nanofibers of conducting polymers at the present time. In this method, macro- or nanoporous membranes are used as templates for nanotube and nanofibers synthesis; and this method has been successfully applied to synthesize polyacetylene [4], polyaniline[5], poly(3-methylthiophene) [6], and polypyrrole [7-11]. The main advantages of the "template synthesis" method is that the length and diameter of the resulting nanostructured conducting polymers could be controlled by the selected nanoporous membranes, thereby, more regular nanostructured conducting polymers can be obtained.

In our previous report [12], we have successfully fabricated a new kind of nanoporous block copolymer thin film, either coating on the silicon wafer or directly on the electrode probes, with thickness only 10 nm to 80 nm. Using this template, we introduce electrochemical polymerization for generating conducting polymer nanomushrooms of PPy on the electrodes in this report. Furthermore, conducting polymer nanohairs of PPy have also been electrochemically deposited on the electrode probe using Nuclepore polycarbonate membranes as templates. The morphologies and electric properties were all extensively investigated.

Experimental

Materials

The present work was carried out in aqueous solutions. Pyrrole (Py) and poly(sodium-4-styrene sulfonate) (PSS) are purchased from Aldrich and used without any prior purification. Two kinds of nanoporous membranes were used as template membranes for the synthesis of nanostructured PPy. Nanoporous block copolymer thin films with an average thickness of 80 nm, and different pore size in diameter ranging from 20 nm to 40 nm were prepared by our procedure [12]. Nanoporous Nuclepore™ polycarbonate track-etched membranes used in this work were supplied by Whatman. Single or four shanks of electrode probes were supplied from the Center for Neural Communication Technology, University of Michigan, Ann Arbor, MI.

Electrochemical Polymerization

A small piece of nanoporous block copolymer thin film was floated on the surface of water, directly transferred to the electrode probes, and let dry at room temperature for at least 24 hours. A layer of about 300 nm of gold was pre-deposited on one side of the Nuclepore membranes using vacuum coating, then stuck onto the electrode probes using Scotch tape. The detailed description of the electrochemical deposition of PPy/PSS on electrode site has been reported in our quarterly reports previously. [2, 12-13]

Electron Microscopy

Scanning electron microscopic images were obtained using high resolution Philips XL30 FEG Scanning Electron Microscope (SEM) with a typical voltage of 5 kV and spot size of 3. For morphologies studies using SEM, the Nuclepore membrane has been dissolved by dichloromethane. A thin film of gold (10~20 nm) was sputtered onto the surface of samples using a Hummer-600 sputtering system to help image the organic film against the silicon background.

Impedances Spectroscopy & Cyclic Voltammetry

The detailed description of the impedance spectroscopy measurements has been reported in our series quarterly reports previously[2, 12-13]. Cyclic Voltammetry (CV) was performed using a house-designed potentiostat, combined with a phase lock amplifier (Stanford Research System

SR 830), personal computer (Gateway 486 DX2/50), multiplexer (National Instruments SC-2062), and Lab VIEW software (National Instruments). The three-electrode cell setup was the same as that used for impedance spectroscopy. A scan rate of 100 mV/s was used and the potential on the working electrode was swept between –0.9 to 0.5 V vs. SCE. These limits were wide enough to include the reversible redox reaction yet narrow enough to avoid over-oxidation and remain within the water window. Before each CV was recorded, several cycles were swept to ensure that the film reached its stable state.

Results and Discussions

Nanoporous Block Copolymer Thin Film

We produced the nonporous block copolymer thin film as a template using block copolymer, poly(styrene-*b*-methyl methacrylate), donated P(S-*b*-MMA), with a molecular weight of PS: 146,700 and PMMA: 70700, and polydispersity of 1.11. The volume fraction of the PMMA was 0.43 [12]. The typical SEM micrographs of nanoporous block copolymer thin films, with ranging from 20nm to 40 nm in diameters of holes, are seen in Fig. 1. After rinsed by acetic acid, the empty PMMA domains were exposed and appeared darker in the micrograph (Fig. 1A). It is evidence that the holes go through the entire film as show from the cross-section (Fig. 1B, shown by white arrows). The characteristics of nanoporous block copolymer are summarized in Table I.

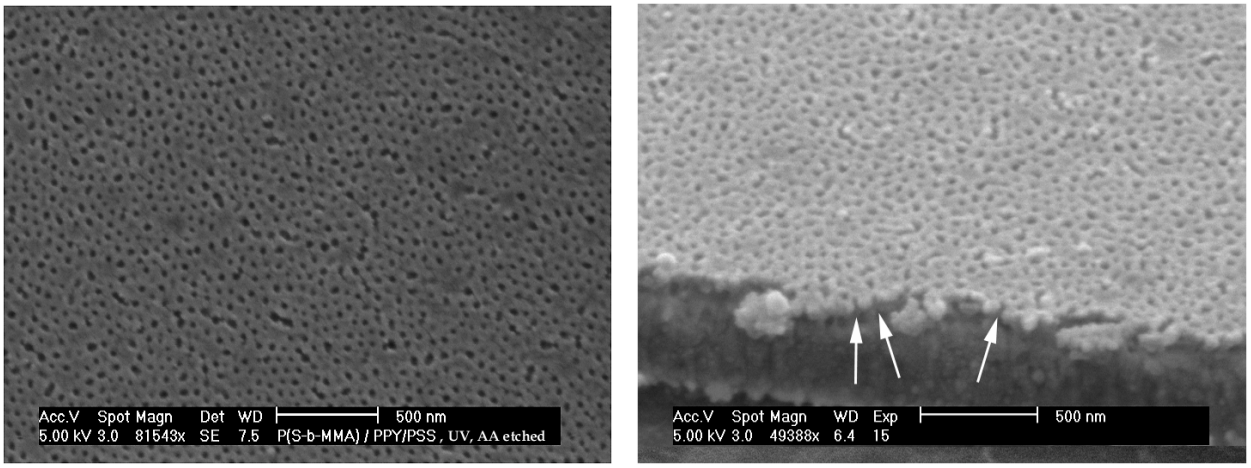

A B

Fig.1. SEM micrographs of hexagonally arrays of holes in gold-coated silicon wafer obtained from an ultra thin film of P(S-*b*-MMA) after removal of the PMMA-block inside the cylinders, A) show a top view, B) a cross-sectional view.

Table 1 Characteristics of Nanoporous Block Copolymer Thin Film

	Block Copolymers
Membrane type	P(S-*b*-MMA)
Membrane diameter (mm)	-
Average of membrane thickness (μm)	0.01~0.08
Pore size (μm)	0.02~0.04
Rated pore Density (pore/cm^2)	-
Porosity (%)	-

In our study, the conducting polymers of PPy/PSS were electrochemical polymerized on the electrode sites with current density of 0.1~0.5 mA/cm^2. A series of SEM images of PPy/PSS deposited on gold-coated wafer as a function of deposition time are shown in Fig. 2. The single nanoscale nodules of PPy/PSS (150nm to 350nm) grow on the surface of nanoporous film, we called this feature as "conducting polymer nanomushrooms". Fig. 3 showed the diagram of conducting polymer nanomushrooms grown on substrate. One hypothesis is that the formation of the nanomushrooms could result from a limited diffusion of the monomer and dopant inside the pores. Indeed, at the beginning of deposition, PPy/PSS was growing in or along the holes. Growth proceeds in the pores until they are filled up to the top surface of nanoporous block copolymer thin film. Beyond this, growth can continue in three dimensions and hemispherical caps form on the top of holes. Since the nanomushrooms are very small as compared to normal nodules seen in our previous work [2, 13], they should increase the surface area of electrode.

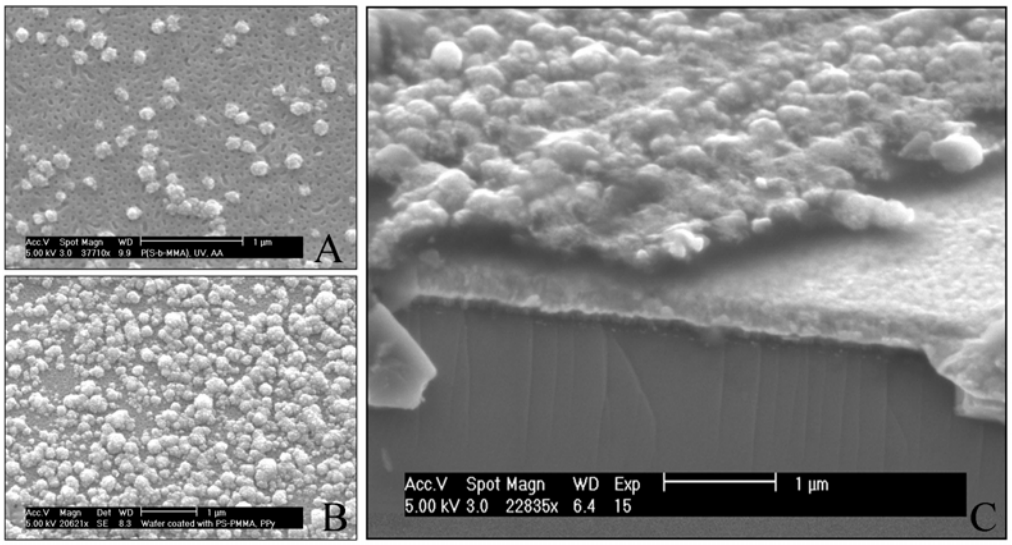

Fig. 2 SEM images of PPy/PSS deposited on the gold-coated wafer with current density of 0.2mA/cm^2 using nanoporous block copolymer thin film as a template. The deposition time: A) 10min, B) 20min, and C) the cross-section views of B.

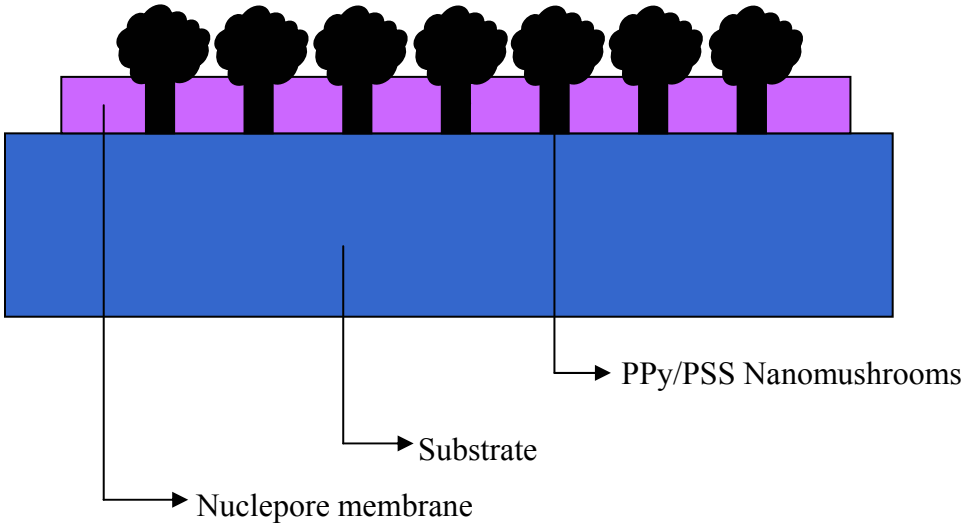

Fig.3. Schematic of conducting polymer nanomushrooms grown on substrate

Furthermore, the nanoporous block copolymer thin films were generated on the single or four-shank electrode probes. Conducting polymer nanomushrooms of PPy/PSS were electrochemically deposited in the holes and come out of the surface of nanoporous block copolymer thin film. The typical SEM images in Fig. 4A show that the nanoporous block copolymer thin film were coated on the whole shank, including the electrode site. Conducting polymer nanomushrooms were only deposited on the electrode site with diameters usually ranging in size from 100 nm to 400 nm, the smallest one is only 50 nm (Fig. 4B)

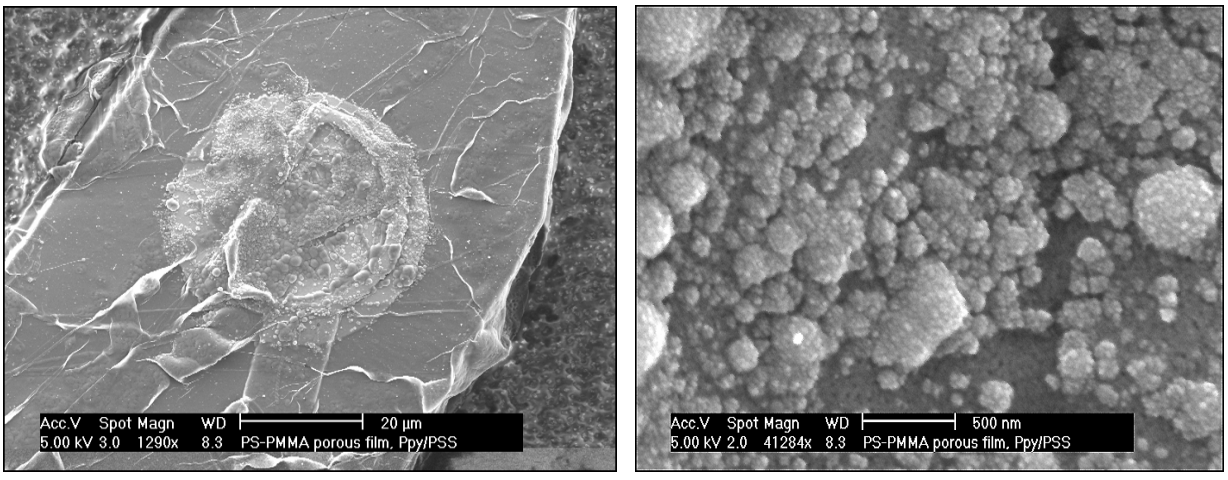

A B

Fig. 4. SEM images of PPy/PSS electrochemical deposited on the electrode site using nanoporous P(S-*b*-MMA) film as template with deposition charge of 3.6µC.
A) One whole electrode site; B: Image at high magnification

The electrochemical deposition method allows for precise control of conducting polymer nanomushrooms growth on the electrode sites. Fig. 5 shows the PPy/PSS nanomushrooms deposited on gold electrode sites with different deposition charge under galvanostatic conditions. The surface area of the electrode is significantly increased by the coating of conducting polymer nanomushrooms.

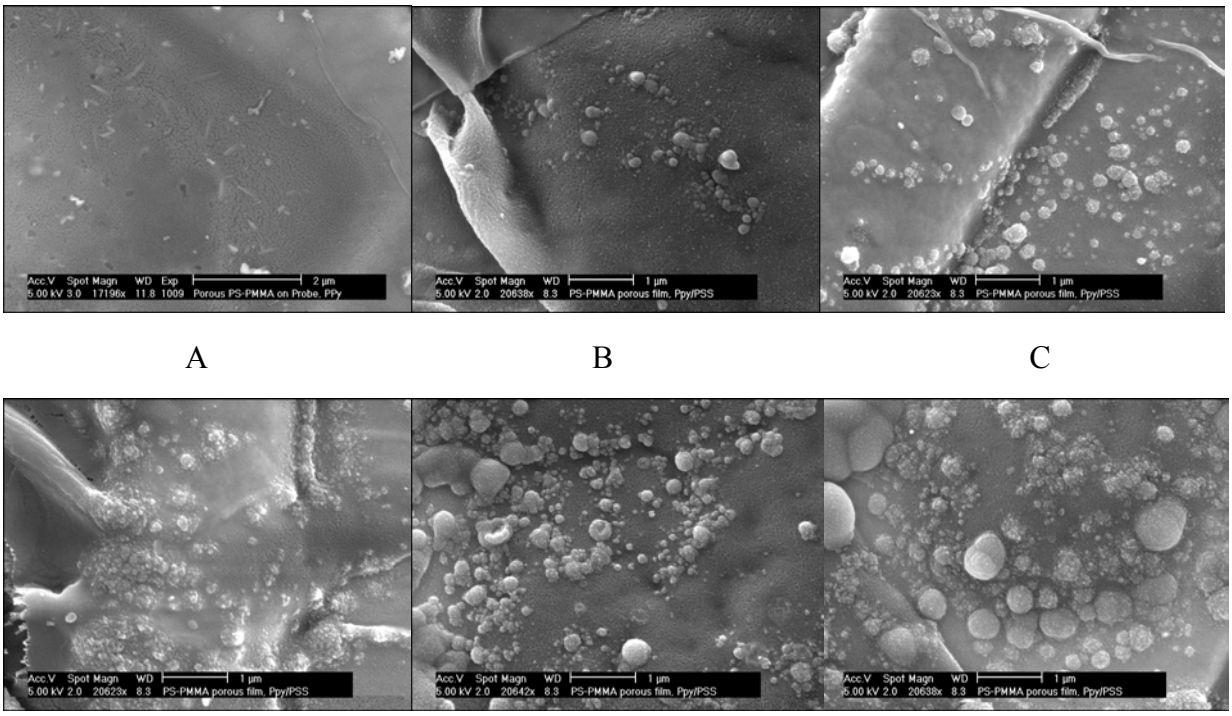

Fig. 5 Nanoporous block copolymer thin film, P(S-*b*-MMA), templated PPy/PSS on the probe as a function of deposition charge:A): 0.1μC; B): 0.3 μC; C): 0.6 μC; D): 1.2 μC; E): 1.8 μC; F): 2.4 μC

Impedance spectroscopy measurements were performed on both uncoated and coated electrodes to examine the electrical properties of the coatings (Fig.6). It was found that impedance magnitude of the conducting polymer nanomushroom coated electrodes (red, solid square) were significantly lower than the uncoated gold electrodes (black, solid circle curve). At 1 kHz, the impedance modulus dropped more than 1 order of magnitude and the phase angle dropped from 80° (black, open circle curve) for gold to 45° (red, open square curve). This significant drop in impedance both in magnitude and phase angle can be partly explained by the increase of the surface area due to the roughened surface morphology at the nanoscale level. The impedance at 1 kHz has been used as a standard measure of the electrode quality, because most of the neural activity is around 0.3~1 kHz. Lowering the impedance without changing the geometric area of the electrode presumably will help to increase the detection sensitivity to neural activity.

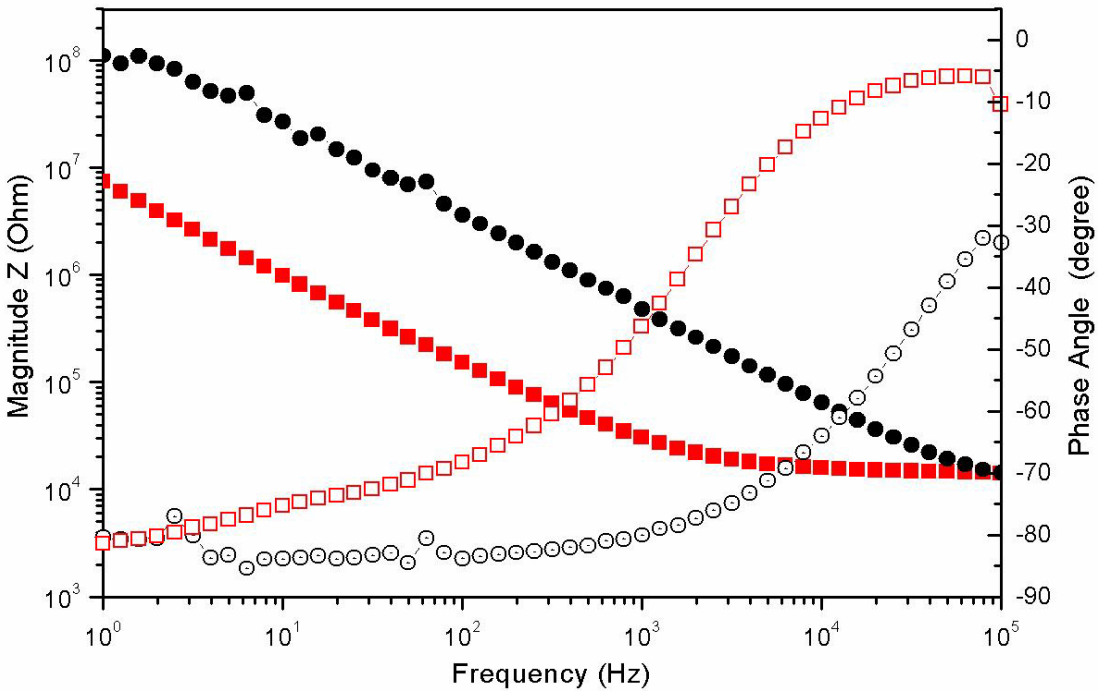

Fig. 6: The impedance spectroscopy of nanoporous block copolymer thin film templated PPy/PSS coated on the electrode site as compared to bare gold electrode. Conducting polymer nanomushromms of PPy/PSS deposited on the gold electrode with deposition charge of 3.6 μC

The electrochemical stability of the conducting polymer nanmushrooms of PPy/PSS coated on the electrode site was tested using CV (Fig. 7). The coatings on the electrode were examined under a potential swept from -0.9 to 0.5 vs. SCE. CV shows the intrinsic redox reaction in the coatings (red curve), as compared to bare gold electrode site (black curve), it has good charge capacity. During the cycle, the film undergoes reduction and oxidation with corresponding movement of ions in or out of the film. In our case, the Na^+ cations move out when the film is oxidized and move in when it is reduced. In addition, we found that the oxidation potential for nanomushrooms of PPy/PSS is around -0.15 V vs. SCE which is much lower than that of normal nodular PPy (0.1 V. vs. SCE) [14]. This lower reduction potential means a higher resistance to any biological reducing agents in the living tissue. This property is highly desirable in chronic implantation of neural probes.

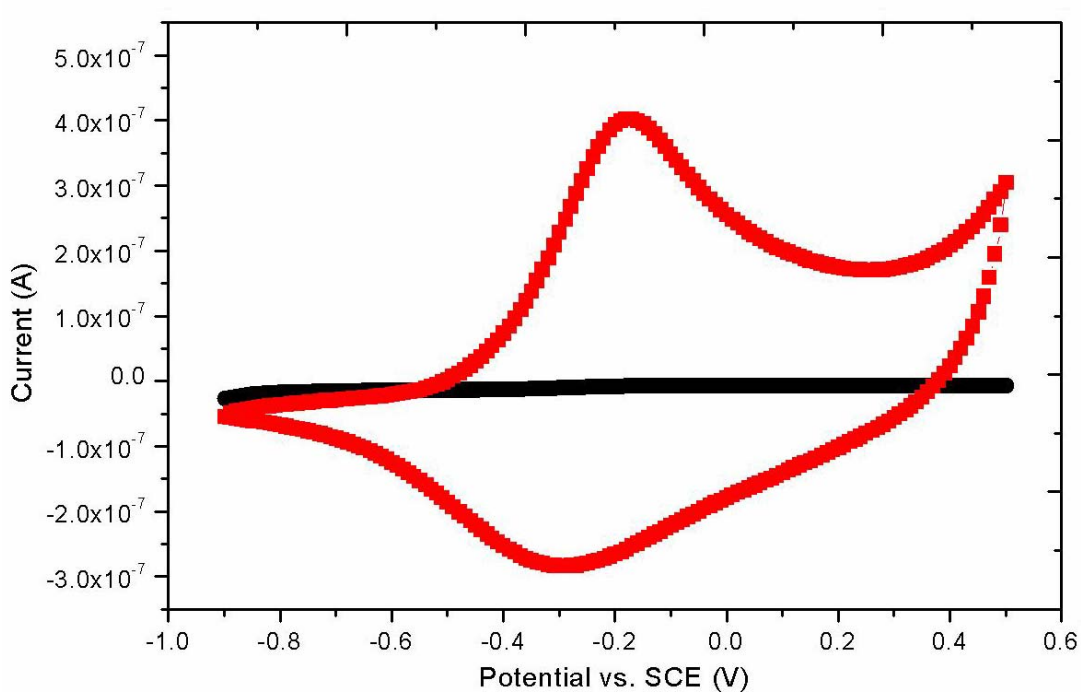

Fig.7 Cyclic Voltammetry of nanoporous block copolymer thin film, P(S-*b*-MMA), templated nanomushrooms Ppy/PSS on Probe

Nanoporous Nuclepore™ Polycarbonate Track-etched Membrane

Two kind of commercial membranes, Anodisc[13] and Nuclepore purchased from Whatman were used as templates in our research. The characteristics of the membranes are listed in Table II.

Table II Characteristics of Commercial Membranes

	Anodisc[13]	Nuclepore
Membrane type	Aluminium Oxide	Polycarbonate
Membrane diameter (mm)	13	25
Average of membrane thickness (μm)	60	6
Pore size (μm)	0.02	0.05
Rated pore Density (pore/cm^2)	-	6x10^8
Porosity (%)	-	<15

In this report, Nuclepore membrane was selected as an example and used as a template to synthesize the conducting polymer nanohairs on the electrode site. The SEM image of Nuclepore membrane is shown in Fig. 8, the diameter of the holes ranged from 40 nm to 50 nm.

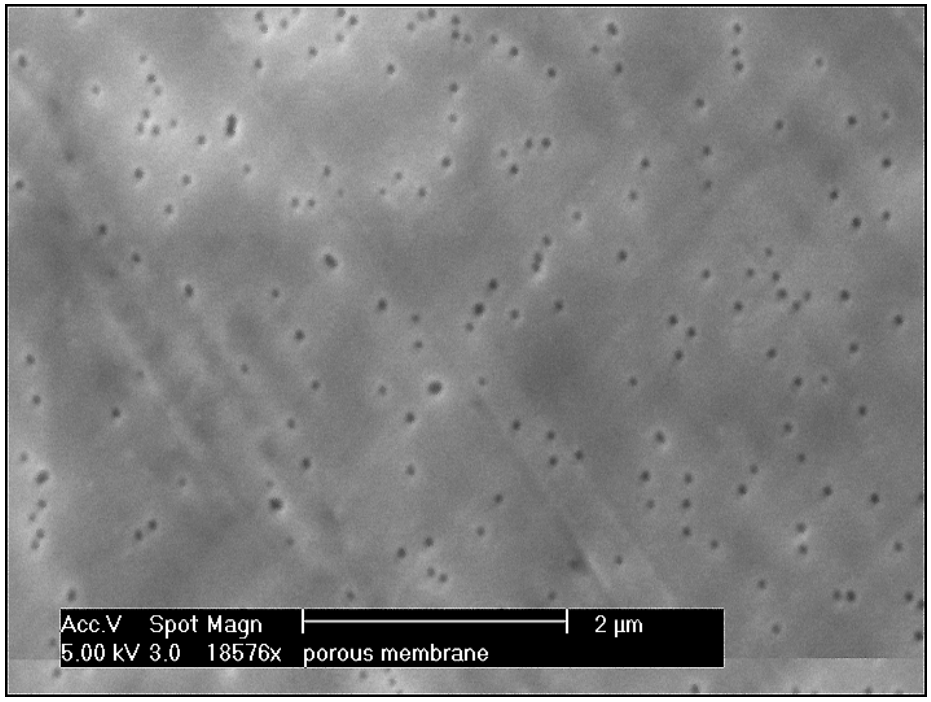

Fig. 8 SEM image of surface morphology of Nuclepore polycarbonate membrane, the pore size is ranged from 0.04 ~0.05 μm

To study the morphology of the PPy/PSS film coated on the electrode using Nuclepore as a template as a function of deposition charge, SEM was used. Fig. 9 shows a SEM micrograph of a gold site coated with PPy/PSS using Nuclepore as a template with fibrillar morphology. From its cross-section view of same sample, we can clearly see that the conducting polymers hairs are standing on the surface of electrode site with diameter about 50 nm (Fig. 10). Since the

PPy/PSS deposited on the electrode site with deposition charge of only 0.1μC, we can only obtain short nanohairs.

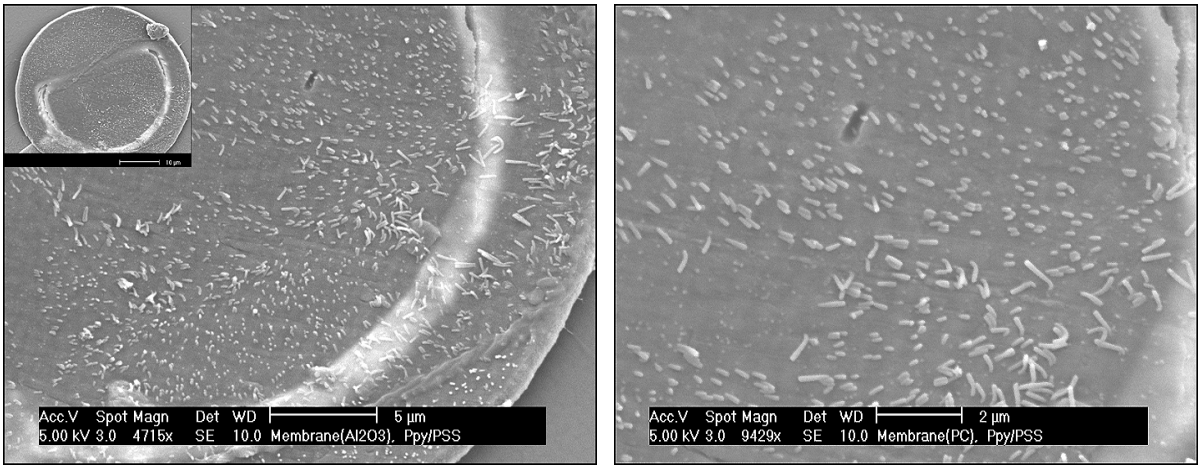

A B

Fig. 9. SEM images of PPy/PSS electrochemical deposited on the electrode site using Nuclepore membrane as a template with deposition charge of 0.6μC. A) One part of electrode site, inset in upper left is whole electrode site; B: Image at high magnification

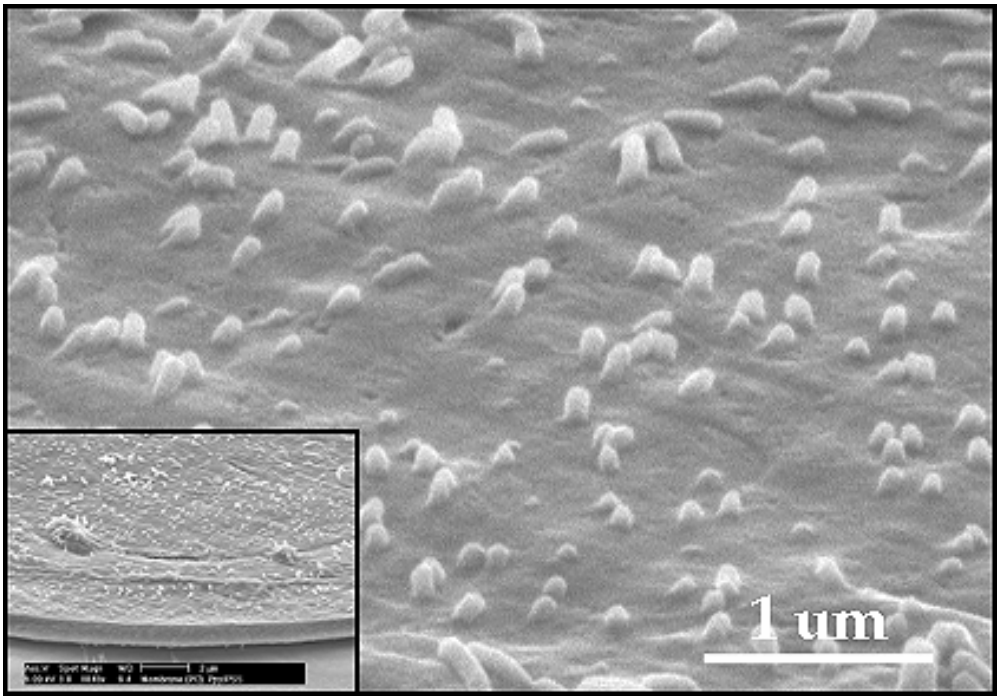

Fig. 10. SEM cross-section images of PPy/PSS nanohairs electrochemicallyly deposited on the electrode site using Nuclepore membrane as a template with deposition charge of 0.6μC. Inset image in lower left is the edge of electrode site.

As compared with the normal nodular morphology of PPy/PSS in our previous work, the conducting polymer nanohairs grown from a neural electrode through nanoporous polycarbonate membranes will result in a coating with extremely high surface area. By increasing the deposition charge at 3.6 μC, a very rough surface with conducting polymer nanohairs morphology on the electrode site has been obtained (Fig. 11).

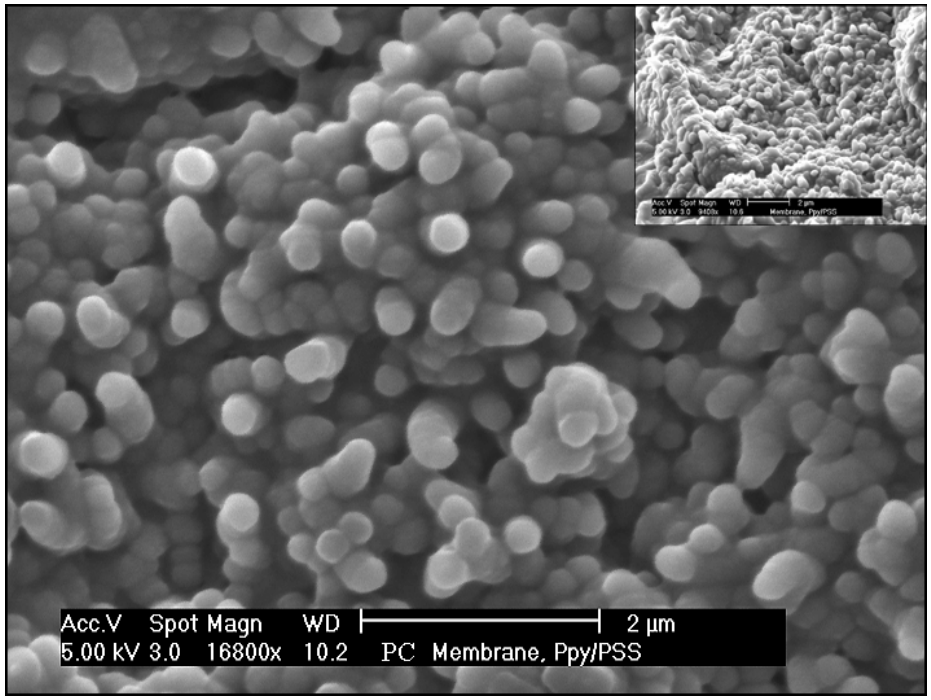

Fig.11. SEM images of Ppy/PSS electrochemical deposited on the electrode site using Nuclepore membrane as a template with deposition charge of 3.6 μC. Inset image in upper right is a cross-section of the same sample.

The electronic and electrochemical properties of nanohairs of PPy/PSS were measured using impedance spectroscopy and CV. As discussed above, we know that the impedance is characterized by a magnitude (|Z|) and phase angle (θ), and is most generally represented as a function of frequency. For a capacitor, the impedance is purely imaginary, which indicates that the current is out of phase with the voltage by 90°. In a resistor, the impedance is real, the current and voltage is in phase and the phase angle is 0°. For a system composed of some combination of these two components, a large phase angle value indicates that the impedance is predominantly capacitive, while small angle values are resistive. Impedance spectroscopy involves measuring the electrode impedance over a spectrum of frequencies. Information about the system under test was obtained by comparing the input signal to the output signal. Magnitude and phase information was measured directly. Using these data, we obtained a qualitative and quantitative idea of the electrical properties of the system over a large range of frequencies and could correlate this information with the morphology of the electrode-medium interface.

Fig. 12 shows the impedance spectroscopy of nanohairs of PPy/PSS coated electrodes (blue, solid circle curve) in comparison with uncoated gold electrodes (black, solid square curve). After being coated with PPy/PSS, the impedance magnitude from 1 to 10^4 Hz was lower than that of the uncoated gold electrode. The phase plot of the impedance spectroscopy showed that the phase was around 80° for gold (black open squares), which meant that the electrode was close to a pure capacitor. After coating with nanohairs of PPy/PSS (blue open squares), the phase decreased to ~15° at 1 kHz, which indicated that the PPy coated electrode was more dominated by its resistive component. Since the surface of nanohairs PPy/PSS was rough and contained a lot of recesses, the electrolyte may have infiltrated into those recesses, making the electrode resistive.

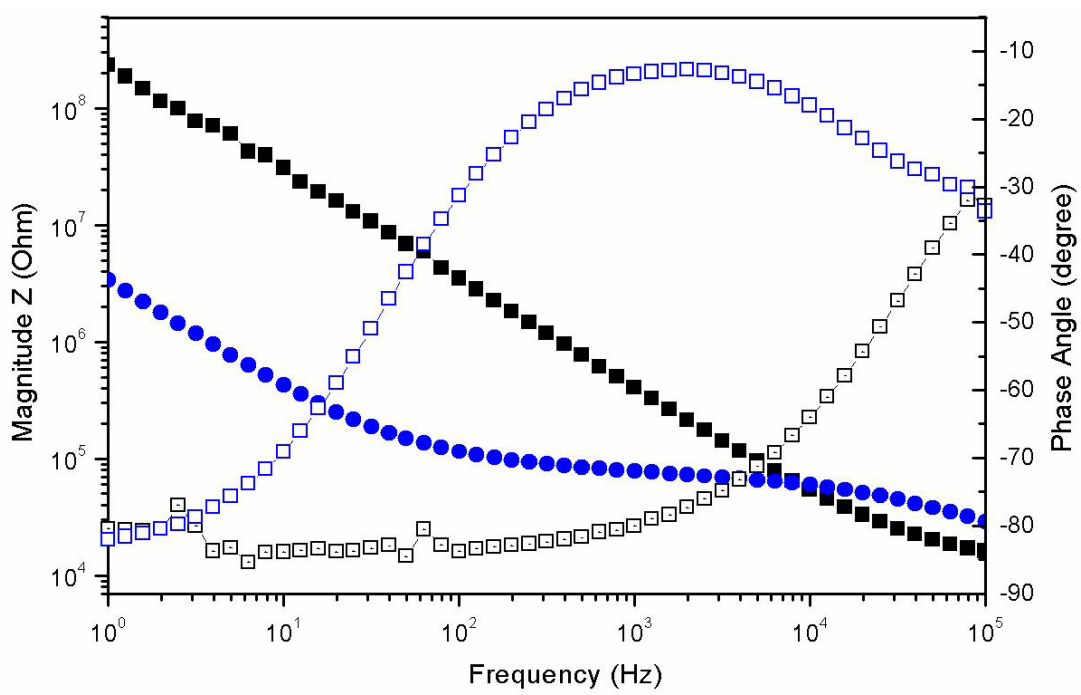

Fig. 12: Impedance spectroscopy of gold sites with (blue) and without (black) nanohairs of PPy / PSS coatings including: magnitude of impedance as a function of frequency (solid symbols), and phase of impedance as a function of frequency (open symbols).

CV provides information about the intrinsic redox reaction of the electrode material as the potential of the electrode is swept in a cyclic manner. Since gold is inert, no redox reactions happen at the gold electrode. Within a single voltage sweep cycle, there were two peaks (one anodic and one cathodic) at potentials of –0.43 and –0.52 V vs. SCE, which were indications of the oxidation and reduction reactions of PPy/PSS respectively. In addition, we found that the oxidation potential for nanohairs of PPy/PSS is around -0.35 V vs. SCE which is much lower than that of normal nodular PPy (0.1 V. vs. SCE) and PEDOT (-0.2 V. vs. SCE) [12]. Again, this lower reduction potential means a higher resistance to any biological reducing agents in the living tissue. This property is highly desirable in chronic implantation of neural probes.

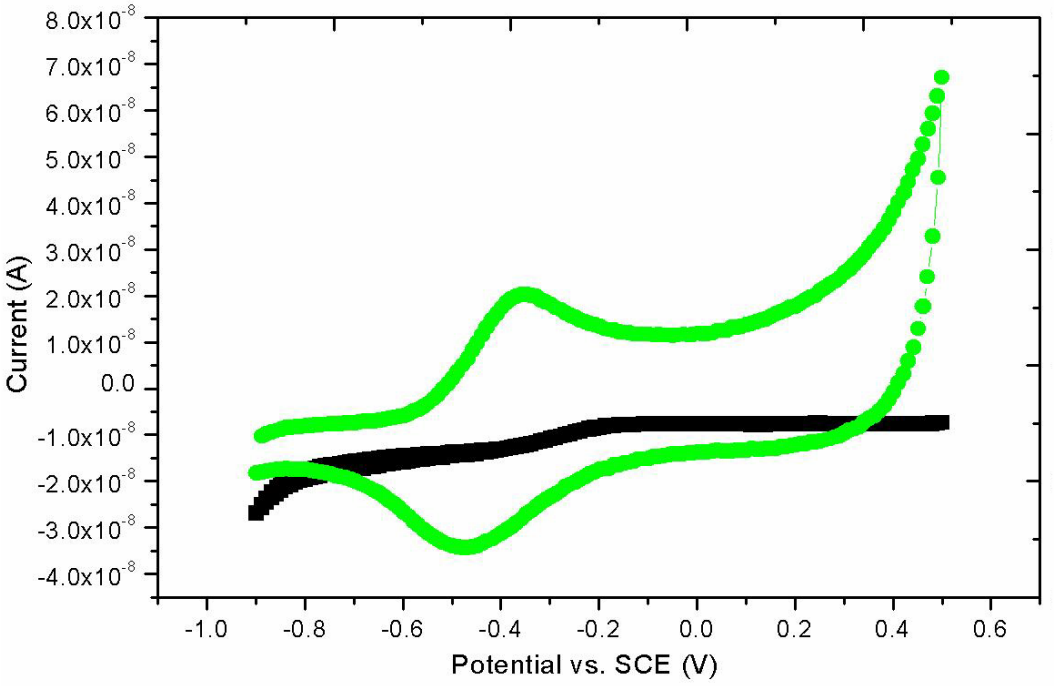

Fig. 13 Cyclic voltammetry of conducting polymer nanohairy PPy / PSS coated site in comparison with uncoated gold sites. The diameter of electrode site is 40 μm. Nanohairy PPy / PSS was deposited on the gold site by passing 3.6 C of charge.

Conclusions

We successfully demonstrate a method to rapidly and reliably fabricate nanostructured conducting polymer coatings (nanomusrooms and nanohairs) on the electrode probes using nanoporous membranes as templates. The coating's thickness, size, length of nanomushrooms and nanohairs can be tailored by changing current density, deposition time , pore size and thickness of templates. The coated electrode has a much high surface area, low impedance and higher stability that will potentially provide a larger efficient interface for signal transport.

Future Work

Conducting polymer with longer hairs will be studied using different porous size membranes as template. Further we will incorporate with bioactive peptide and then do *in vivo* controlled release of neurotrophic factors.

References

1. Xinyan Cui, Valerie Lee, Yehoash Raphael, James Wiler, Jamie Hetke, David, J. Anderson,and David C. Martin, *Journal of Biomedical Materials Research*, Vol 56, n2, 261-272 (2001)
2. Quarterly Progress Report #I, January 30 (2002)
3. C. R. Martin, *Science*, 266,1961 (1994)
4. W. Liang, C. R. Martin, *J. Am. Chem. Soc*., 112, 8976 (1990)
5. Z. Cai, J. Lei, W. Liang, V. Menon, C.R. Martin, *Chem. Mater*., 3, 960 (1990)
6. Z. Cai, C.R. Martin, *J. Am. Chem. Soc*., 111, 4139 (1989)
7. C. R. Martin, *Adv. Mater,* 3, 457 (1991)
8. J. Mansouri, R. P. Burford, *J. Membrane Sci*., 87, 23(1994)
9. S. Demoustier-Champagene, P. Stavaux, *Chem. Mater*., 11, 829(1999)
10. J. M.Mativetsky, W. R. Datars, *Solid State Communication*, 122, 151 (2002)
11. S. V. Ermolaev, N. Jitariouk, A. L. Moel, *Nuclear Instruments and Methods in Physics Research B*, 185, 184(2001)
12. Quarterly Progress Report #III, July 31 (2002)
13. Quarterly Progress Report #II, April 30 (2002)
14. Xinyan Cui, Ph.D Thesis (2002)

Electrochemical Deposition of Polypyrrole in Alginate Hydrogel Coatings

Our techniques for creating conducting polymers inside hydrogels were refined as described in this section. The data indicates that the pyrrole can be deposited near the electrode on the hydrogel as a scaffold. We also found that at high current rates, undesirable results occur: the polymerization becomes unstable and propagates along the hydrogel-probe interface.

Experimental

1- Alginate coating on the surface of probes

Materials

Alginate powder Pronova MPG was provided from Biopolymers Inc. Calcium Sulfate was purchased from Sigma.

Preparation of hydrogel

Alginate was dissolved in distilled water (1g/100ml) under stirring conditions for 20 hr. Also 0.5 of Calcium sulfate was dissolved distilled water for 20 min. Alginate solution was gelled and cross-linked around of the shanks of probes by dipping method. The thickness of alginate coated could be controlled by number of dips inside the alginate solution. In this study, hydrogel thickness was 30-60 μm.

2- Electrochemical Deposition of PPy

First of all, PSS was dissolved in distilled water (0.1M). Then 0.2M Py and 10 ml of calcium solution were added to the PSS solution and was followed by stirring condition for 2 hr. After preparation of final solution Py monomers were polymerized on the surface of electrode sites and was grown inside the hydrogel structure by electrochemical deposition apparatus in galvanostat mode in different time and current density. The growth of PPy was studied by Optical Microscopy.

Results

Pyrrole monomers were polymerized on the electrode sites at the current of 6 nA for 10 and 20 minutes under galvanostatic (controlled current) conditions. The growth of PPy in hydrogel structure at the different times of deposition is shown in the following figures.

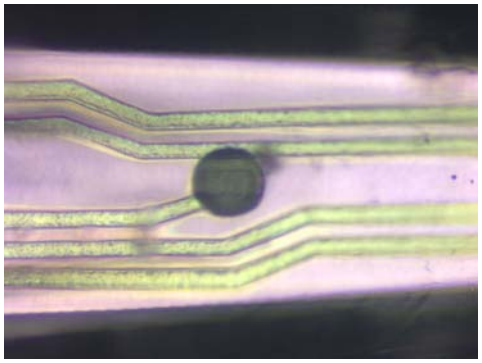

I = 6 nA , t = 10 min (top view)

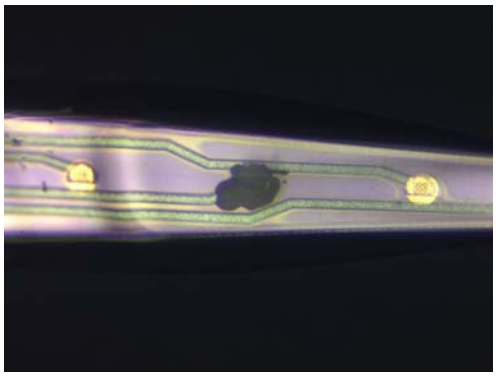

I = 6 nA , t = 20 min (top view)

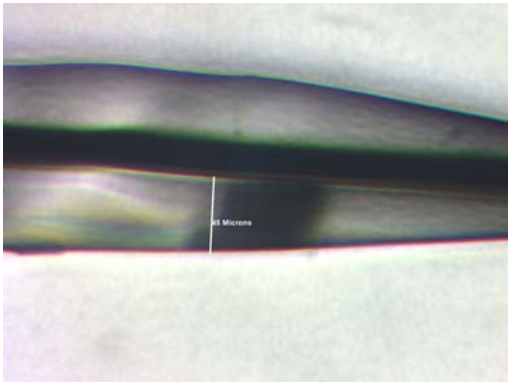

I = 6 nA , t = 20 min (lateral view)
Thickness = 45 µm

By increasing the current of electrochemical deposition to 20 nA the Py was polymerized at the surface of aliginate hydrogel layer. This is generally an undesirable result, although there may be reason to consider surface-restricted polymerizations for certain applications or future probe designs.

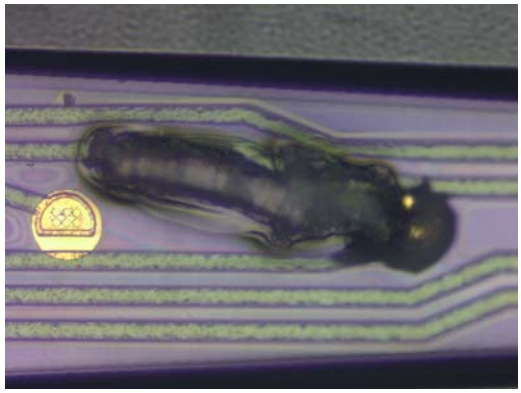

I = 20 nA, t = 20 min

The degree of reswelling of the dehydrated hydrogel in the monomer solution was changed with the amount of $CaCl_2$. The figure shows the change in impedance as a function of polymerization time, and as a function of dehydration. The value of the impedance of these probes at 1 kHz was the lowest after 40 minutes of polymerization, with a value of 7 kΩ. This is the lowest value of impedance that we have yet observed (Fig 1). The hydrogels were placed in the monomer solution for 10 min to allow the hydrogel to reswell to its original shape. The 40 min (dehydrated in the Fig. 1) shows the impedance of the samples measured before reswelling. The impedance of the dehydrated sample was similar to that of the hydrated sample in the low frequency range. However, the impedance of the dehydrated sample was much higher than hydrated one in the high frequency range. These differences evidently reveal the important role of the local environment (density of the coating) in limiting charge transport to the probe.

Fig1. Impedance Spectroscopy of Pyrrole/PSS Grown in the Hydrogel: Ohms vs. Hz

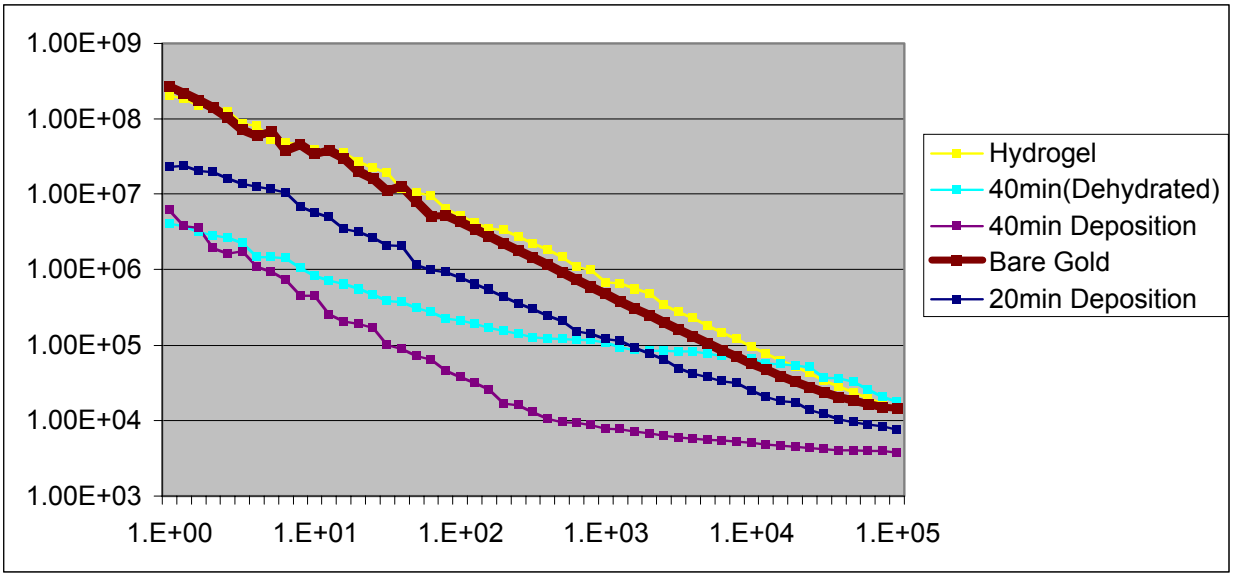

However, to allow neovascularization and ingrowth of the neurons into the hydrogel layers, the pore size of the hydrogel which was made of the MVG alginate may not sufficient. We have investigated lyophilized hydrogels which have much larger pore size than that of intact hydrogels, and have examined how these modified hydrogels act as a scaffold of polymerization of the conducting polymers.

In this session, the preparation and characterization of a three-dimensional porous hydrogel is described for creating a sufficient space to allow ingrowth of axons. This porous hydrogel is prepared by a three-step procedure (Shapiro and Cohen, Biomaterials, 18, 583-590, (1997)). Firstly, gelation of the alginate with $CaCl_2$, followed by freezing of the hydrogel and finally lyophilization to produce a porous hydrogel. The pore size was controlled by changing the freezing temperature. In this study, liquid nitrogen (-198 ^oC) and a conventional refrigerator freezer (-20^oC) were used for solidification of the hydrogel. The composition of the alginate used in this study was varied as shown in Table 1.

Concentration of Alginate soution	Freezer	Liquid Nitrogen
1wt%	-20 ^oC	-180 ^oC
1.5wt%	-20 ^oC	-180 ^oC
2wt%	-20 ^oC	-180 ^oC

Table 1.

Briefly, sodium alginate was dissolved in double distilled water, to a final concentration of 1-2%. 5 ml of the alginate solution was crosslinked with calcium ions by adding 0.2 ml of 8.4g/40ml calcium sulfonate solution by syringe method. Freezing was accomplished by either placing the hydrogel in a -20°C freezer, or by submerging them into liquid nitrogen (-196°C). The frozen plates were immediately transferred to vacuum vessels and lyophilized at <10 mbar until dry.

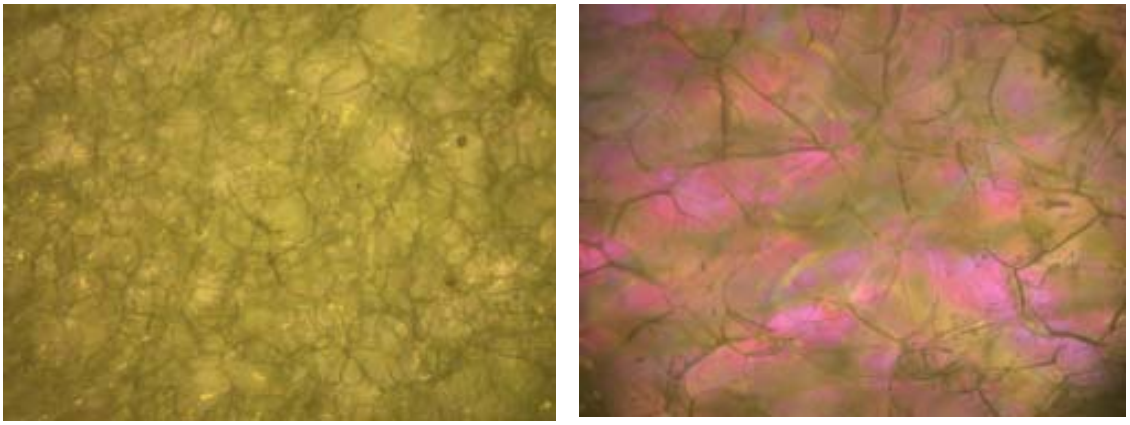

Fig 2. (a) A lyophilized hydrogel by freezer-freezing (b) A lyophilized hydrogel by liquid N_2-freezing

The dried hydrogels prepared by different freezing temperatures displayed different pore morphology, as judged by the optical images.

The conducting polymer grown in the macroporous hydrogel scaffolds show substantially different morphologies from that obtained in a homogeneous hydrogel. Fig 3(b) shows the conducting polymer which was grown in the freezer-frozen hydrogel. In contrast to the conducting polymer in the intact hydrogel (Fig3(a)), the conducting polymer in the lyophilized hydrogel (Fig3(b)) is more densely concentrated around the electrode. This could be explained the larger pore size of the hydrogel allowing more pyrrole monomer to diffuse into the electrode easily. There was not much difference found between the morphology of the polypyrrole grown on the freezer-frozen hydrogel and liquid N_2-frozen hydrogel. This evidently means that the pore size of the hydrogel caused by either method of freezing is large enough to allow the pyrrole monomer to readily diffuse into the hydrogel.

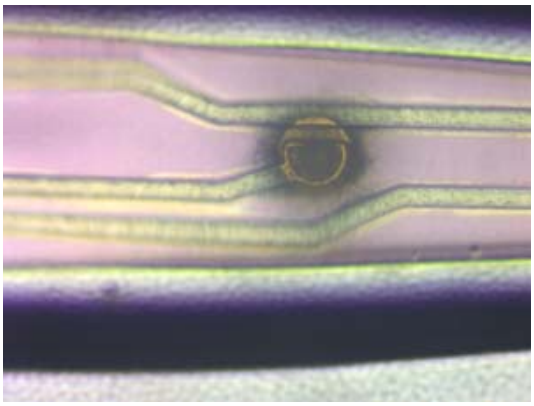

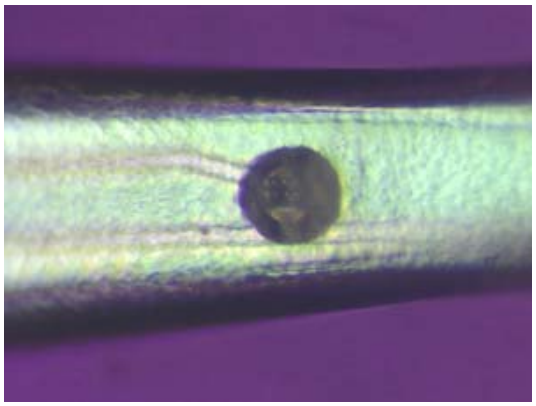

Fig 3a: Polypyrrole grown in the intact hydrogel. The external boundary of PPy is diffuse, and the gold electrode can be easily seen on the probe surface. Fig 3b: Polypyrrole grown on the frozen-porous hydrogel. The boundary is more distinct, and the gold electrode can no longer be seen as clearly.

From the lateral view of these samples it is clear that in contrast to the conducting polymer grown in the intact hydrogel (Fig.4(a)), the conducting polymer in the lyophilized hydrogel grows more straight forward to the surface instead of spreading out around the electrode.

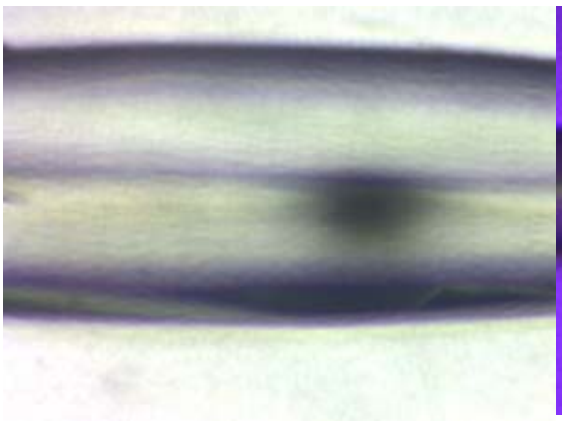

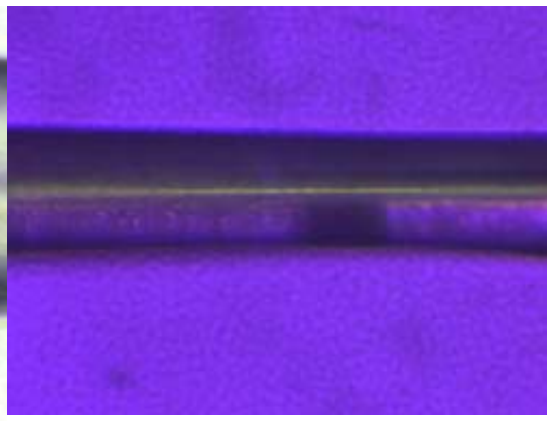

Fig. 4(a) Lateral view of the conducting polymer in the intact hydrogel Fig. 4(b) Lateral view of the conducting polymer in the lyophilized hydrogel.

Quarterly Progress Report for the period August – October, 2002
Report #4, October 31, 2002

Keck Center for Tissue Engineering
Patrick A. Tresco, P.I.
University of Utah subcontract for N01-NS-1-2338

Overview

The current report summarizes continuing progress on the characterization of the brain wound healing response to intracortical microelectrode arrays. Included is an analysis of relative abundance and distribution of neurofilament expression adjacent to single shank 16 channel microelectrode arrays implanted in the cerebral cortex. This was assessed by indirect immunoflouresent methods and analysis with laser scanning confocal microscopy. We provide evidence that the density of neurofilament-positive fibers is reduced in the parenchyma immediately adjacent to microelectrode arrays and that the reduction occurs by one week and is sustained at two weeks; a timeframe over which many arrays experience loss of single unit recording.

Technical refinements in the use and application of a lipophilic dye for tracing of the implantation tract of single shank microelectrode recording arrays is presented and discussed. In addition, we introduce a method for objective and unbiased quantification of the brain tissue response that extracts relative fluorescent intensity values along predetermined lines drawn perpendicular to the implant interface to compare the relative intensity of cell-type specific antigens from histological sections. This approach will be employed for all future comparisons of host response at different time points and with respect to different coatings.

Technical Refinement of Microelectrode Array Implantation Tract Tracing

The location of the microelectrode array implantation tract can be difficult after it has been withdrawn from the perfused and fixed brain tissue. To solve this problem, we previously described a method for using the lipophilic tracing dye, $DiIC_{18}(3)$ (DiI) that was applied as a small volume of concentrated solution to the pial surface and through which the microelectrode was lowered during implantation into the brain tissue. The approach was effective at labeling the implantation tract but tended to be diffuse in adjacent brain tissue, especially in sections near the surface of the brain. While effective in localizing the micorelectrode implantation tract, the amount of fluorescent labeling was more than what was needed, was variable and lowered our ability to resolve differences in the relative intensity of other fluorescent reagents. To build upon the technique and limit the amount and spread of dye within the microelectrode tract, we have immobilized dye on the microelectrode surface using a simpe dip coating procedure. Microelectrode arrays were immersed in a solution of

$DiIC_{18}(3)$ (5 mg/mL in ethanol,removed and allowed to air dry in a laminar flow hood. The process was repeated 5 times for each electrode. Evaporation of the dye on the microelectrode surface produced a layer of adherent crystals. Implantation of such DiI-coated microelectrodes yielded a more compact and less intense fluorescence signal in the tract (representative outcome-Figure U4-1). A variety of time points were analyzed from 1 week through 4 weeks. All demonstrated effective labeling of the tract, and in addition appeared to which to resolve individual fibers in the vicinity of the implant that presumably came in contact with the microelectrode either during or after insertion. Furthermore, sufficient dye is carried by the implant as dye labeling was evident through the entire depth of the implant dorsal to ventral or from the shaft to the tip containing the recording sites. As a result, this approach will be employed in all future implantation studies.

Unbiased quantitative analysis of tissue response to implanted materials

We have developed a method for collecting a series of line-based intensity profiles from captured digital images. The fluorescence intensity of any stained section can be quantified and expressed as mean pixel intensity as function of distance from the implant interface. Using this approach it is possible to compare the host response as a function of any given variable using standard and objective criteria that can be compared with statistical methods. Serial brain sections are first collected. For any desired immunostain, a series of evenly distanced sections are batch stained using the same solutions sand conditions and mounted. Images of immunostained sections are viewed and captured by a PMT device mounted on a laser scanning confocal microscope. Images are stored as unsaturated 8 bit TIF files. For any given session where many images are captured, the same acquisition settings are used (PMT voltage, scan time, capture resolution, laser intensity, etc.). The settings are determined so that all images are of sufficient brightness for viewing, but the vast majority of pixels are not saturated. Single optical sections are collected and stored for each sample. During any given capture session, a control image is also collected as an intensity reference. In this manner, intensity profiles for any given session can be pooled and/or compared with profiles taken from another session by normalizing all intensities to their respective controls. The control consists of a slide containing a homogenous suspension of the same conjugated secondary antibody used for immunostaining the analyzed tissue sections (in this instance Alexa 488 labeled goat antibody). The control is viewed and captured with identical settings applied to stained sections. Thus for any given capture session, all intensity values can be normalized to control.

To ensure non-biased intensity profile developed at the Keck Center for Tissue Enginering that uses three points to delineate a reference arc at the interface of an implant. The angular location and size of the reference arc is adjustable

enabling exclusion of defects that may be present in image such as air bubbles. Once a reference arc is delineated intensity sampling profiles are generated at a density of ~1.7 deg/profile and will yield 20-35 profiles per image analyzed (Figure U4-2). Profiles extend normal to the delineated arc and are radially indexed in 0.5μm increments. At each radial increment an anti-alias pixel extraction algorithm is applied to derive an intensity value based on a weighted averaging of pixels in nearest proximity. A single image intensity profile is then calculated by averaging all coinciding increments of the sampling profiles generated and is performed simultaneously for all color channels (RGB) present in images. The average image intensity profile along with its radial indices is then saved in a text format file for later numerical analyses. Following profile analysis of all experimental group images, an average probe intensity profile can be calculated for each of the sample groups and probes utilized.

Figure U4-2. Radial line sampling of relative fluorescent intensity of a digital image. A horizontal section of a hollow fiber membrane whose lumen was loaded with a Texas-Red labeled lysine fixable dextran.

This method is currently being applied to a catalog of images taken from the existing stained specimens derived from untethered and tethered implants at various time points up to 12 weeks, and will be employed where relevant for all subsequent analyses. In the following section, we present our analysis of spatial changes in neurofilament intensity adjacent to microelectrode implant tracts at various time points.

Neurofilament Organization Adjacent to Implanted Microelectrodes

Materials and Methods:

Electrode Preparation, Implantation, and Tissue Preparation*:* The data presented includes histological analysis of single uncoated untethered 16 channel microelectrode arrays. All procedures were performed as described in earlier reports.

Immunostaining: The relative abundance and distribution of neurofilament was determined by incubating sections with a monoclonal antisera against the 160 kDa neurofilament (Clone NN18; Sigma) at a dilution of 1/500. Visualization of the reaction product was conducted with a fluorescently labeled secondary as previously described

Image Acquisition: Images were acquired with an Olympus Fluoview confocal microscope from horizontal tissue sections and with identical PMT settings and scan times. Single XY optical sections were collected at 1024x1024 resolution and stored as 8 bit TIF files.

Intensity Profiling: Images were loaded into a Labview analysis program. An arc was delineated along the implant tissue interface created by the retrieved microelectrode array. Twenty radial line profiles were generated as depicted in the illustration in Figure U4-2 and all subsequent data was exported to a text file. Data for each time point and condition were pooled and the average pixel intensity at each distance increment was generated.

Results and Discussion:

Examination of neurofilament organization around the retrieved microelectrode array implantation tract revealed a reduction in filament density immediately adjacent to the site occupied by the electrode when compared to the relative intensity in the adjacent parenchyma in the same section (Figure U4-3). The decrease in neurofilament distribution formed a radial zone of extending to a distance occupied by two to three neuronal cell bodies away from the implant site. The reduction of staining appeared to result form loss of neuronal bodies in the reactive zone. This pattern was observed at all time points and appeared similar in animals implanted with tethered microelectrode arrays. However, such an analysis of tethered implants has proven to be difficult due to the poorly defined implantation tract margins, and the increased background or non-specific staining associated with the presence of blood products and tissue macrophages, both of which are auto-flourescent. The relative intensity of radial line profiles shows neurofilament reactivity as function of distance from the implant interface at as early as 1 week and 2 weeks (Figure U4-4), indicating a reduction in neurofilament intensity within a 20 microns radius of the implant interface tha tis reduced at 1 week and remains reduced at 2 weeks. Such a reduction has been noted over longer implant periods in the rabbit (Edell et al.,

1992); however, given its limited perimeter, little functional consequence has been attributed to this change. Interestingly, the reduced neurofilament density in this zone is coincident with an accumulation of OX-42 reactive microglia/macrophages (Figure U4-5). As we have previously discussed, this accumulation and the formation of a strongly adherent compact layer on the electrode surface could represent a significant impedance layer and a potential source of neurotoxic factors. This together with a reduced abundance of proximal targets, as is indicated by our current findings, may represent underlying mechanisms for loss of unit recording that have been reported with use over this time frame. Whether the reduction in relative abundance and distribution of neurofilament changes at time periods greater than 2 weeks and whether the relative changes are affected by tethering to the skull will be addressed

Future Work

We intend to expand the quantitative assessment of tissue response for each the various markers employed, and where possible perform a complete statistical analysis of the tissue response between tethered and untethered microelectrode arrays. In addition, we expect to have early time point data on a brain tissue response to a number of surface coatings in our next report.

References:

Edell, D.J., Toi, V.V., McNeil, V.M., and L.D. Clark. 1992. Factors influencing the biocompatibility of insertable silicon microshafts in cerebral cortex. IEEE Trans. Biomed. Eng. **39**: 635-643.

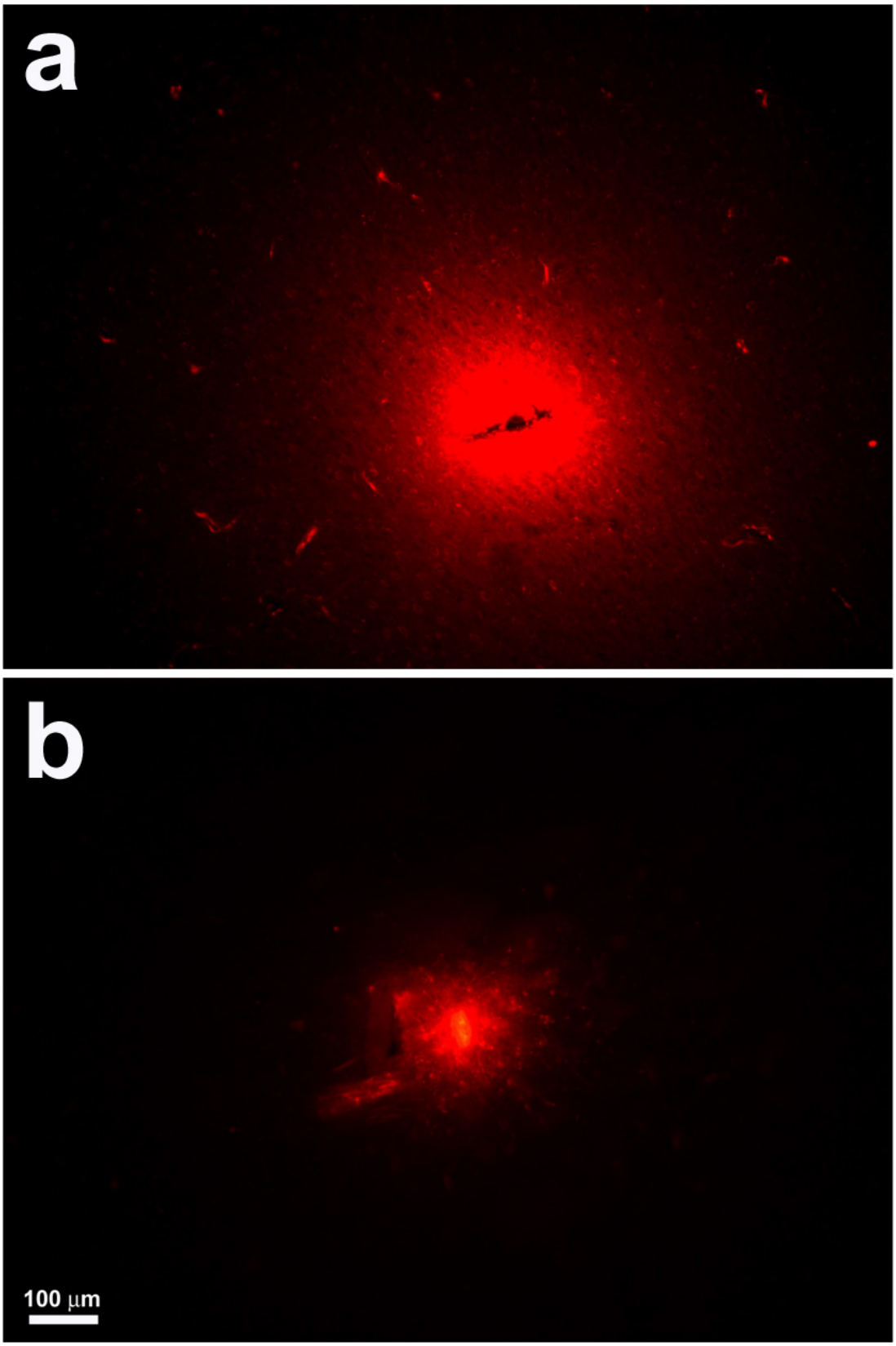

Figure U4-2. Tracing the electrode path by dip-coating electrodes in DiI. A comparison of cortices treated with a solution of DiI at the brain surface (a) or implanted with an electrode previously dip-coated with DiI. Coating the electrode produces a more compact and less intense spread of dye. Both photos are taken from horizontal tissue sections at 1 week post implantation.

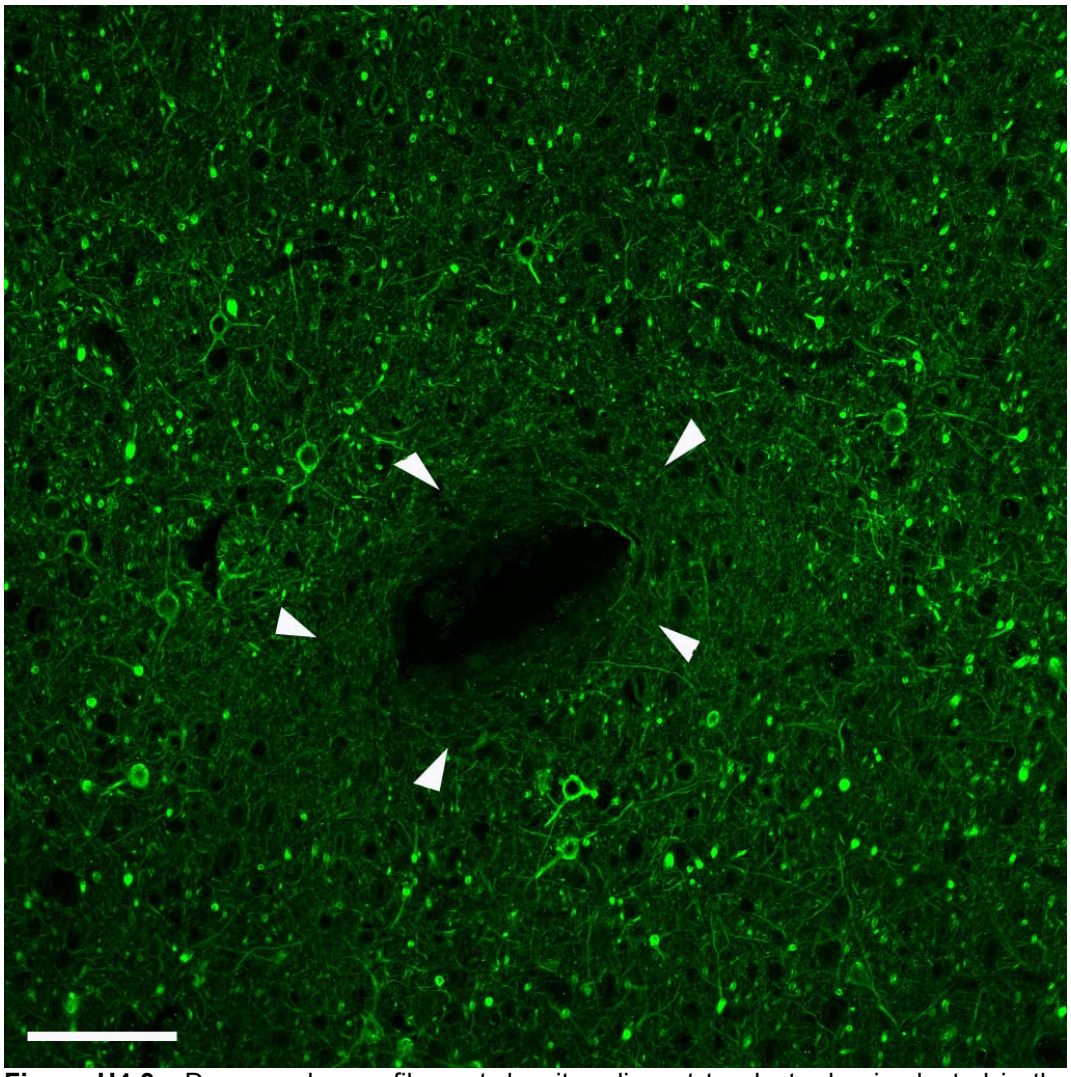

Figure U4-3. Decreased neurofilament density adjacent to electrodes implanted in the cerebral cortex. A representative image from an animal implanted for 1 week with an uncoated untethered acute microelectrode. Arrows demarcate the radial zone of reduced neurofilament staining relative to the surrounding parenchyma. Scale bar = 100 microns.

Figure U4-4. Neurofilament intensity as a function of distance from implant interface. Shown are profiles for 1 week and 2 week for single shank 16 channel uncoated, untethered microelectrode arrays. Vertical bars represent standard deviation about the mean intensity of each distance interval. 20 line profiles were generated from each of at least 6 images per time point.

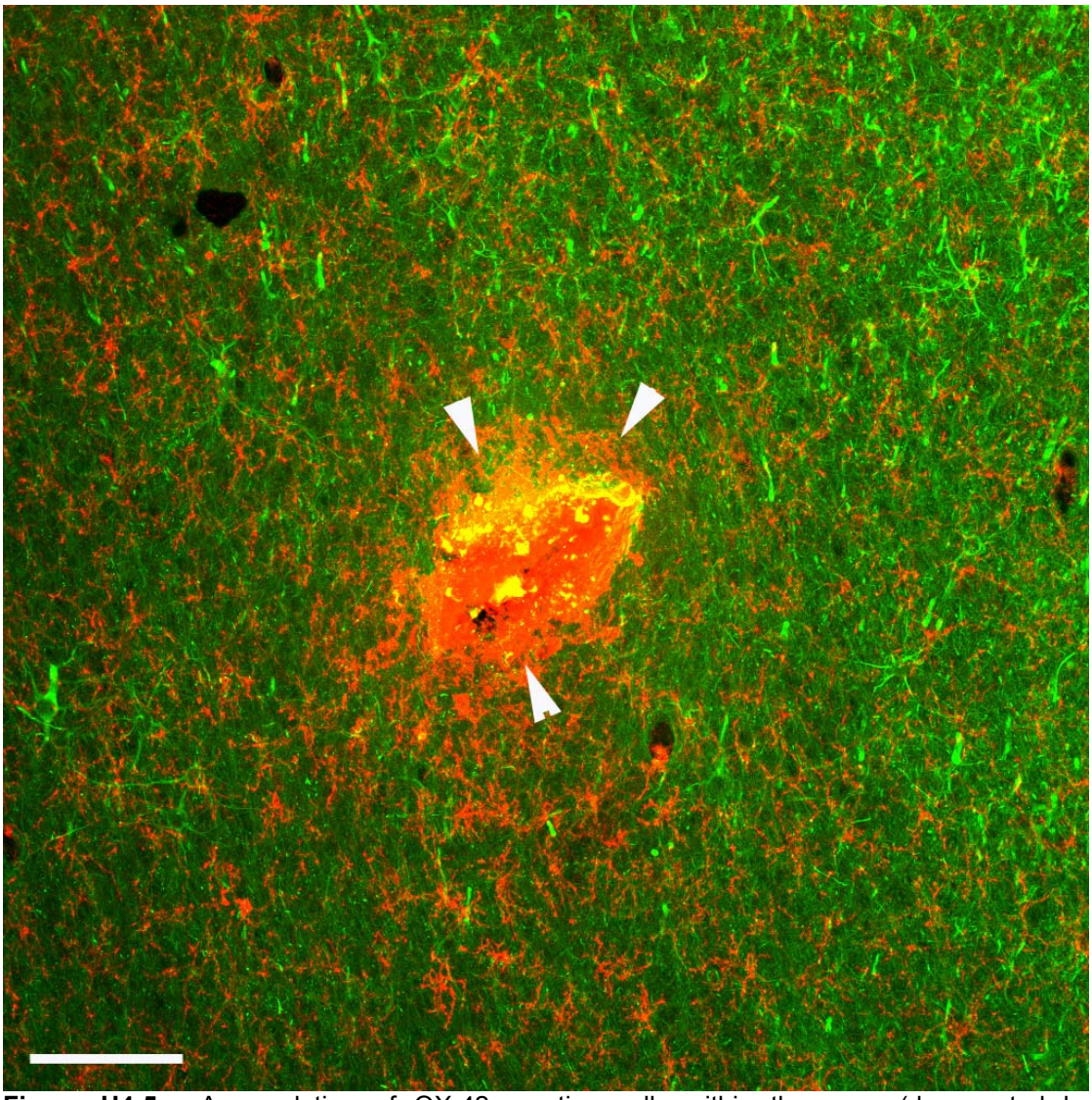

Figure U4-5. Accumulation of OX-42 reactive cells within the zone (demarcated by arrowheads) of reduced neurofilament density. Representative image from a horizontal tissue section at the level of the cerebral cortex through the implantation tract of a retrieved single shank 16 channel untethered uncoated microelectrodearray at 1 week. Neurofilament (green), OX-42 (red). Scale bar = 100 microns.